Progress In Electromagnetics Research M, Vol. 71, 51–61, 2018

Waveguide Designing for Absorbing Modulator in GaN/AlN Structure for All Optical Networking

Ali Rahmani[1] and Ali Rostami[2, 3, *]

Abstract—In this paper a waveguide is introduced as an absorbing modulator using GaN/AlN structure based on spherical quantum dots. The role of waveguide (modulator) dimensions on optical profile of light in the channel and coupling efficiency is also investigated. These parameters can affect the main characteristics of modulator like absorption and depth of modulation. First we will give a brief explanation about the all optical modulator structure based on spherical quantum dots and its optical properties. Then the electrical fields in optical fiber and modulator will be introduced, and the effects of dimensions on these fields will be discussed. The results show that the electric field distribution determines the insertion loss and also effects on modulation. Finally we will determine the proper dimensions of modulator for coupling to optical fiber.

1. INTRODUCTION

It is not a long time that optoelectronic and photonic devices based on III-nitride compounds have been known as a useful approach in infrared wavelength applications. This is due to their high ability in high power and temperature resulting from their hardness and large band offset. Recently, III-nitride applications in the infrared region and optical communication windows have been considered in many fields such as detecting, optical processing and switching. Because of strong electron-LO phonon and highly polar material and hence fast decay rate of carriers (sub-picoseconds lifetimes) in intersubband transitions for GaN and AlN quantum wells, they have many applications in optical switching and detecting. Also due to their large conduction band offset $\sim$ 1.7 ev these materials are used in optical communication networking specially in near-infrared wavelengths and 1550 nm window [1–4]. Other compound materials used in communication wavelengths are InGaAs/AlAsSb [5] and (CdS/ZnSe)/BeTe [6] in which GaN and AlN have specific use for their hardness and highly power consumption. Both of them are grown using molecular beam epitaxy (MBE) or metalorganic vapour phase epitaxy (MOVPE) methods in a thin film formation on silicon or sapphire substrates. Of course, using devices based on quantum dot is more prevalent than that based on quantum well. This is due to some advantages of quantum dots specifics. One is the simplicity of quantum dots fabrication process, while growing the quantum wells needs some exact and sensitive techniques of MBE to create sharp steps which increase the cost and time. Between the various shapes of quantum dots, spherical quantum dots due to their cheap and easy synthesis are very attractive for optical device manufacturing. Also because of their high symmetry, normal incidence is allowed. High three-dimensional confinement, low noise and high dipole matrix element are some advantages for quantum dots. Since GaN and AlN have high refractive index and other benefits such as mature, scalability and high versatility on different substrates, they are proper candidates for fabrication in optical waveguide circuits. Also, vast

Received 7 May 2018, Accepted 10 July 2018, Scheduled 24 July 2018

* Corresponding author: Ali Rostami (rostami@tabrizu.ac.ir).

[1] Department of Electrical Engineering, Science and Research Branch, Islamic Azad University, Tehran, Iran. [2] Photonics and Nanocrystal Research Lab. (PNRL), Faculty of Electrical and Computer Engineering, University of Tabriz, Tabriz, Iran. [3] School of Engineering-Emerging Technologies, University of Tabriz, Tabriz, Iran.

transparency window 0.35–13.5 μm for GaN and more than 0.2 μm for AlN make these materials as proper candidates for waveguide applications. Low losses and good guiding properties are important for their operation as high efficiency waveguide structures. Reaching high bitrate and bandwidth is one of the main points in optical and quantum device based on intersubband transitions which has taken a lot of works [7–10]. This is due to low decay rate which we try to compensate by using electromagnetically induced transparency (EIT) technique to transmit carriers from higher to ground state in the four-level system. Also inserting an internal AlN barrier in GaN quantum well interferes with increasing the dipole moment matrix which leads to higher linear susceptibility and finally absorption and depth of modulation [11]. In this study, after presenting a brief explanation about the device structure, the light profiles in fiber and waveguide will be extracted, and then coupling efficiency will be calculated. Finally, the effect of modulator dimensions on its operation and properties will be presented, and proper dimensions will be determined.

2. MATHEMATICAL BACKGROUND

According to our last work [12], to analyze the behavior of all-optical modulator and extract the electronic and optical properties of this device based on multilayer spherical quantum dots in AlN/GaN structure (Fig. 1), we used self-consistent solution of Schrodinger and Poisson equations considering effective mass approximation regard to slowly varying envelope in spherical coordinates. Schrodinger equation in spherical coordinate after many mathematical manipulations is:

$$r^2\frac{d^2R}{dr^2}+2r\frac{dR}{dr}+\left\{\frac{2m_i^*}{\hbar^2}[E-V_i(r)]r^2-\ell(\ell+1)\right\}R=0. \tag{1}$$

Angular quantum number ℓ is defined as: $\ell=0$, so that the transitions are in S subshell. Since electric field stress and strain are high in Wurtzite structures in III-nitride compounds, the effects of piezoelectric and spontaneous polarization and also exchange potential due to exchange correlation are added to the total potential. In the modulator structure shown in Fig. 2, the wells are GaN, since the electron should be in ground state under equilibrium conditions, the barriers chosen from n-doped AlN. After creating the 4-level structure and inserting pump, probe and also control signal to apply electromagnetically induced transparency (EIT) to enhance the modulator speed (Fig. 3), the corresponding time evolution density matrix equations for four-level system is considered as [12]:

$$\begin{aligned}
\dot{\rho}_{11}&=-\frac{i\Omega_{12}}{2}\left(\rho_{12}e^{i\Delta_{12}t}-\rho_{21}e^{-i\Delta_{12}t}\right)+\gamma_{21}\rho_{22}+\gamma_{31}\rho_{33}+\gamma_{41}\rho_{44}.\\
\dot{\rho}_{22}&=-\frac{i\Omega_{23}}{2}\left(\rho_{23}e^{i\Delta_{23}t}-\rho_{32}e^{-i\Delta_{23}t}\right)-\frac{i\Omega_{12}}{2}\left(\rho_{21}e^{-i\Delta_{12}t}-\rho_{12}e^{i\Delta_{12}t}\right)+\gamma_{32}\rho_{33}-\gamma_{21}\rho_{22}-\gamma_{24}\rho_{22}.\\
\dot{\rho}_{33}&=-\frac{i\Omega_{23}}{2}\left(\rho_{32}e^{-i\Delta_{23}t}-\rho_{23}e^{i\Delta_{23}t}\right)-\frac{i\Omega_{34}}{2}\left(\rho_{34}e^{-i\Delta_{34}t}-\rho_{43}e^{i\Delta_{34}t}\right)-\rho_{33}(\gamma_{32}+\gamma_{31}+\gamma_{34}).\\
\dot{\rho}_{44}&=-\frac{i\Omega_{34}}{2}\left(\rho_{43}e^{i\Delta_{34}t}-\rho_{34}e^{-i\Delta_{34}t}\right)+\gamma_{34}\rho_{33}-\gamma_{41}\rho_{44}+\gamma_{24}\rho_{22}.\\
\dot{\rho}_{12}&=-\frac{i\Omega_{12}}{2}\left(\rho_{11}-\rho_{22}\right)e^{-i\Delta_{12}t}-\frac{i\Omega_{23}}{2}\rho_{13}e^{i\Delta_{23}t}-\frac{\rho_{12}}{2}\left(\gamma_{21}+\gamma_{24}\right).\\
\dot{\rho}_{23}&=-\frac{i\Omega_{23}}{2}\left(\rho_{22}-\rho_{33}\right)e^{-i\Delta_{23}t}+\frac{i\Omega_{12}}{2}\rho_{13}e^{i\Delta_{12}t}-\frac{i\Omega_{34}}{2}\rho_{24}e^{-i\Delta_{34}t}-\frac{\rho_{23}}{2}\left(\gamma_{32}+\gamma_{31}+\gamma_{21}+\gamma_{34}+\gamma_{24}\right)\\
\dot{\rho}_{24}&=\frac{i\Omega_{23}}{2}\rho_{34}e^{-i\Delta_{23}t}+\frac{i\Omega_{12}}{2}\rho_{14}e^{i\Delta_{12}t}-\frac{i\Omega_{34}}{2}\rho_{23}e^{i\Delta_{34}t}-\frac{\rho_{24}}{2}\left(\gamma_{24}+\gamma_{21}+\gamma_{41}\right)\\
\dot{\rho}_{34}&=-\frac{i\Omega_{34}}{2}\left(\rho_{33}-\rho_{44}\right)e^{i\Delta_{34}t}+\frac{i\Omega_{23}}{2}\rho_{24}e^{i\Delta_{23}t}-\frac{\rho_{34}}{2}\left(\gamma_{32}+\gamma_{31}+\gamma_{34}+\gamma_{41}\right)\\
\dot{\rho}_{31}&=-\frac{i\Omega_{12}}{2}\rho_{32}e^{i\Delta_{12}t}+\frac{i\Omega_{23}}{2}\rho_{21}e^{i\Delta_{23}t}+\frac{i\Omega_{34}}{2}\rho_{41}e^{i\Delta_{34}t}-\frac{\rho_{31}}{2}\left(\gamma_{32}+\gamma_{31}+\gamma_{34}\right)\\
\dot{\rho}_{41}&=\frac{i\Omega_{34}}{2}\rho_{31}e^{-i\Delta_{34}t}-\frac{i\Omega_{12}}{2}\rho_{42}e^{i\Delta_{12}t}-\frac{\rho_{41}}{2}\left(\gamma_{41}\right)
\end{aligned} \tag{2}$$

Here, $\Delta_{12}=\omega_{12}-\nu_{12}$, $\Delta_{23}=\omega_{23}-\nu_{23}$ and $\Delta_{34}=\omega_{34}-\nu_{34}$ denote the detunings related to pump, probe and control signals. Also γ_{21}, $\gamma_{31}\gamma_{34}\gamma_{24}$ and γ_{41} are relaxation rates. Consequently, to reach the

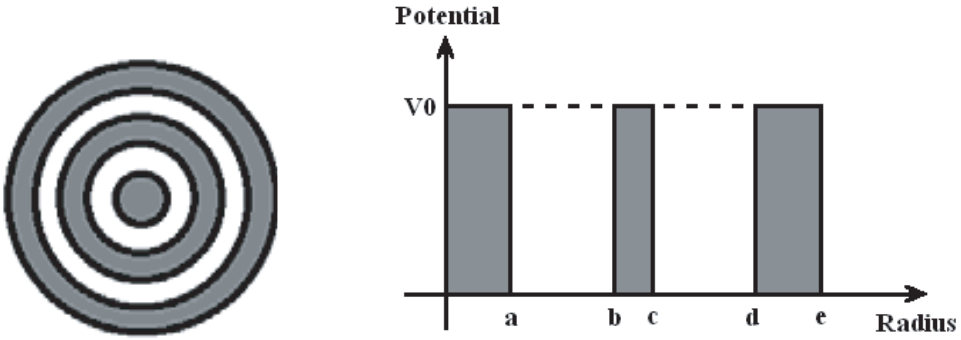

Figure 1. (a) Two-dimentional profile for a multilayer spherical quantum dot and (b) related potential profile along the QD radius [12].

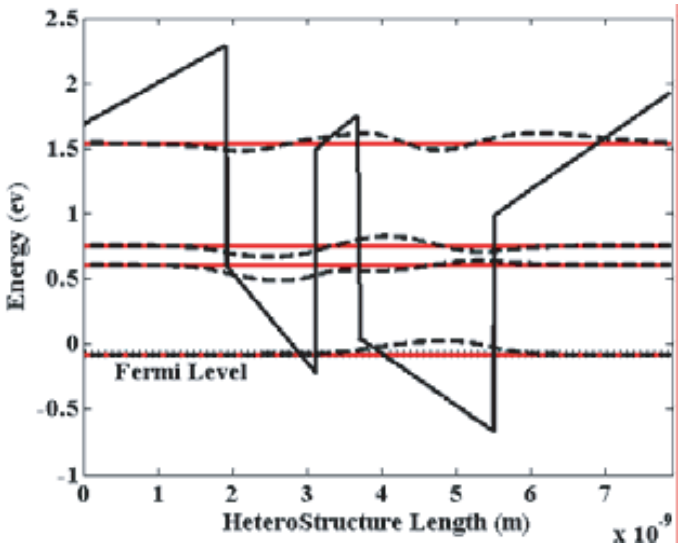

Figure 2. Energy diagram of spherical quantum dot structure in conduction band along the QD radius. (The barriers are from n-doped AlN and the wells are GaN) [12].

absorption, transmission and modulation depth, the linear susceptibility is calculated. The absorption is related to the imaginary section of linear susceptibility. All the equations, flowchart, tables and related items were presented in detail in our last work [12].

$$\chi = \frac{P}{\varepsilon_0 E} = \frac{2N_a \wp^2 \rho_{23}}{\varepsilon_0 \Omega_{23} \hbar} \tag{3}$$

In this modulator probe signal is modulated by the variation of carriers population in state $|2\rangle$. In other words, pump light changes the electrons population in this state and modulates the probe through absorption process. The important characteristic of this device in contrast to its rivals [7–10] is its ultrafast operation due to applying EIT method to conduct the carriers to state $|4\rangle$ and finally to ground state with fast decay. All three lights, i.e., pump, probe and control are applied to a four-level system as shown in Fig. 3 and tuned on 1480 nm, 1570 nm and 1324 nm, respectively. Regarding the high effect of confinement factor in modulator operation, the normal amount for every tenfold layer of quantum dots is $\Gamma = 0.015$ and the QD layers repetition number as: $N = 95$ [13]. Considering transmission matrix method (TMM), the extracted reflection for this structure is $R = \%10$.

Insertion loss is an important parameter in the waveguide structure which is due to the coupling loss of optical systems. In order to obtain this value, first the input coupling should be calculated, and for

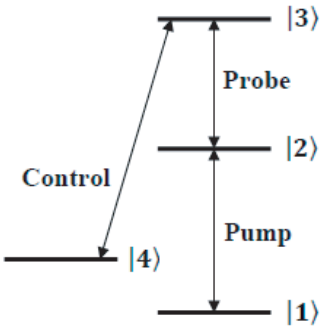

Figure 3. Proposed four-Level system equivalent to quantum dot modulator structure [12].

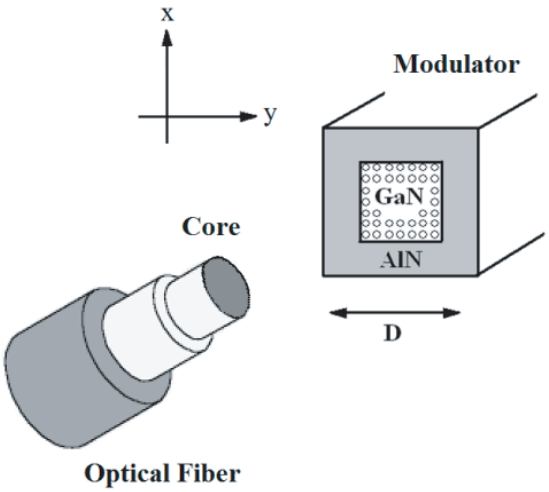

Figure 4. Schematic of optical fiber and modulator (waveguide) structure, (quantum dots are located in GaN core in the waveguide).

this purpose the distribution of the electric field in optical fiber and modulator must be obtained. The overall geometry of the structure is shown in Fig. 4. By calculating the amount of optical coupling (η) between the two elements, the insertion loss can be calculated. With extracting the fiber and waveguide fields and calculating their overlap integral, the optical coupling will be calculated [14, 15]. If ψ_1 and ψ_2 are the field equations in fiber and modulator, the optical coupling is as follows, and consequently insertion loss is: $IL = 1 - \eta$

$$\eta = \frac{\iint \psi_1 \psi_2^* dxdy}{\left(\iint \psi_1^2 dxdy\right)^{1/2} \left(\iint \psi_2^2 dxdy\right)^{1/2}} \tag{4}$$

3. SIMULATIONS AND RESULTS

In order to evaluate the modulator performance and behavior, the values for variables are as follows: the probe beam intensity is equal to 1 mw, i.e., $I_{\text{probe}} = 1.7 \times 10^3$ (Wcm^{-2}) and tuned on 1570 nm, the pump intensity as: $I_{\text{pump}} = 5 \times 10^8$ (Wcm^{-2}) and the intensity of the control signal $I_{\text{control}} = 1.2 \times 10^2$ (Wcm^{-2}). The carrier density: $N_a = 8 \times 10^{18}$ (cm^{-3}) and temperature is: $T = 300$ K. The number of repetitions of the layers of the quantum dots is assumed: $I_2 = 1.5 \times 10^8$. The carrier relaxation rate and surface density of dots are considered equal to: $\hbar\Gamma = 30$ mev and $N = 3 \times 10^{11}$ (cm^{-2}). The

electric fields profile in the fiber and waveguide according to the corresponding equations are obtained based on the physical characteristics of the structure and boundary conditions. In this structure, the refractive indices of doped Sio_2 as the core and cladding of the optical fiber are respectively equal to $n_1 = 1.46$ and $n_2 = 1.45$, and the fiber core radius is equal to $a = 5\,\mu m$. Assuming optical fiber in the form of a single-mode fiber with a step refractive index, the obtained light field in fiber is the first kind Bessel function [15]. The Marcatili's method was also used to calculate optical profile in the waveguide with step refractive index [14, 15]. In this analysis, in accordance with the previous figure, the quantum dots are located in the GaN channel with refractive index $n_1 = 2.3$ and are enclosed by a layer of AlN with $n_2 = 2.2$. Also, the width (W) and height (T) of the waveguide are considered equal ($W = T$). Taking into account E^x_{pq} (TM-like mode in modulator, the electric field profile for fundamental mode in fiber in the first kind Bessel is shown in Fig. 5(a). Also the light profiles in modulator for different dimensions, i.e., $x = y = 1,\ 5,\ 10\,\mu m$, are shown in Figs. 5(b), (c), (d). In the modulator in Fig. 5(b) with dimension of $x = y = 1\,\mu m$, the light field is almost uniform, and by increasing the waveguide dimension to $x = y = 5\,\mu m$ and $x = y = 10\,\mu m$, the field profile decreases and reaches to near zero at the corners of the waveguide (Figs. 5(c), (d)).

Computing the overlapping integrals associated with these two fields and assuming the displacement distance (D) as the displacement in one of the x or y directions between the fiber and modulator

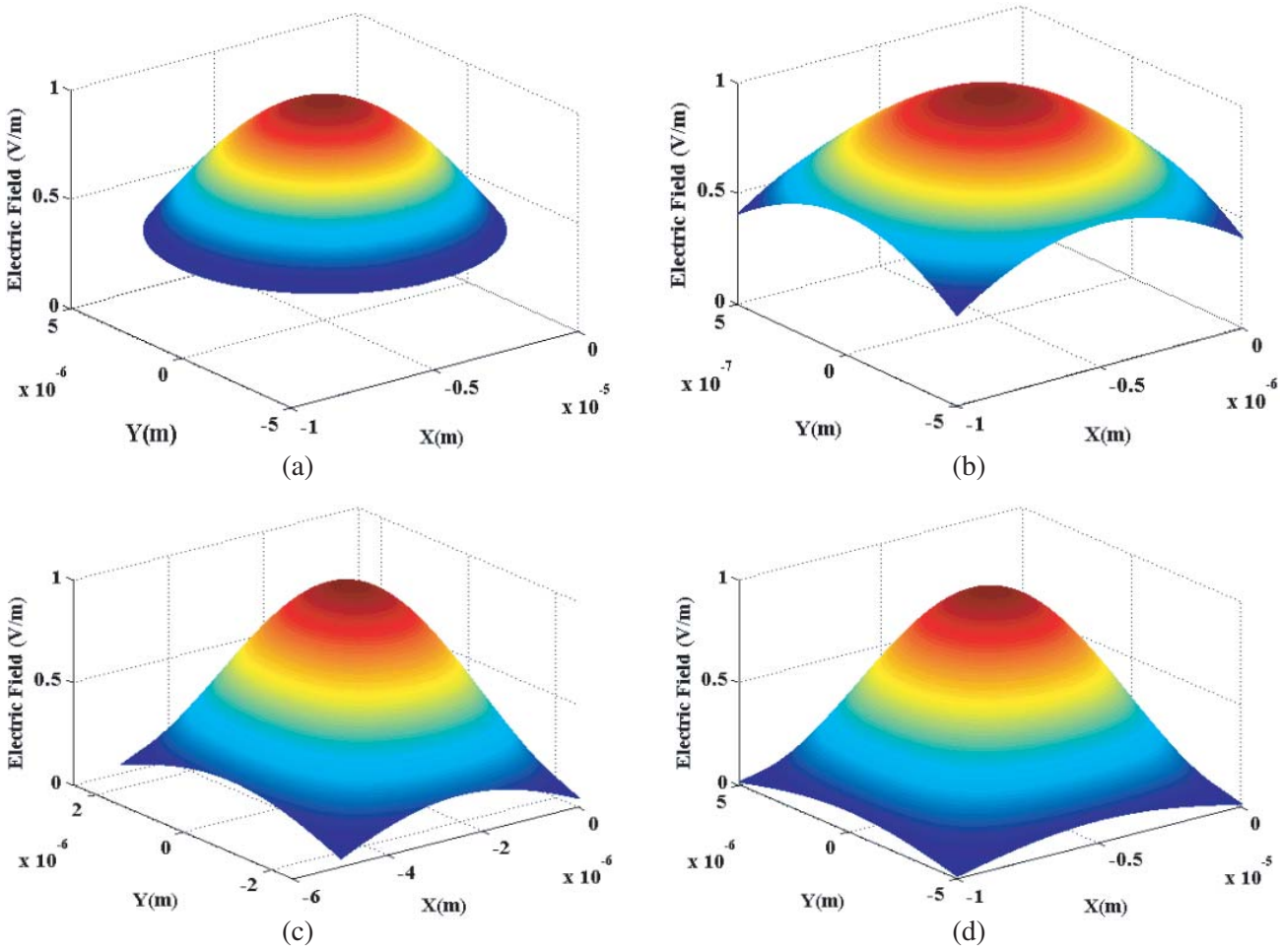

Figure 5. Electric field profile for (a): optical fiber with radius $a = 5\,\mu m$ and modulator with dimensions: (b) $x = y = 1\,\mu m$, (c) $x = y = 5\,\mu m$, (d) $x = y = 10\,\mu m$, refractive index of core and cladding for optical fiber are $n_1 = 1.46$ and $n_2 = 1.45$ and for waveguide are $n_1 = 2.3$ and $n_2 = 2.2$ respectively.

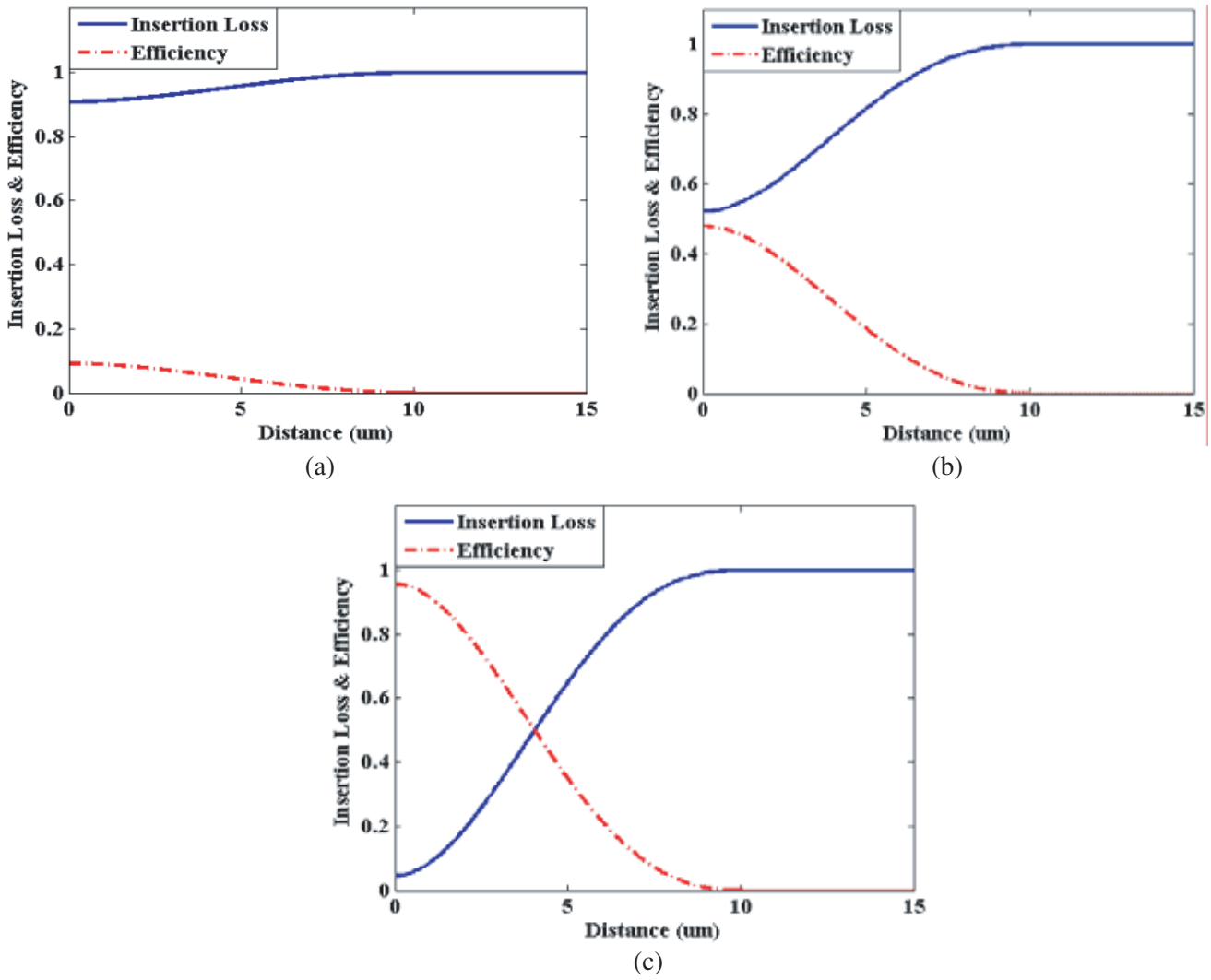

Figure 6. Input coupling efficiency and insertion loss vs. displacement distance between fiber with radius $a = 5\,\mu m$ and modulator for different dimension: (a) $x = y = 1\,\mu m$, (b) $x = y = 5\,\mu m$ and (c) $x = y = 10\,\mu m$, refractive index of core and cladding for optical fiber are $n_1 = 1.46$ and $n_2 = 1.45$ and for waveguide are $n_1 = 2.3$ and $n_2 = 2.2$ respectively.

(mismatching), the input coupling efficiency and the insertion loss in terms of the displacement distance for the different dimensions of the waveguide are displayed in Fig. 6.

It is seen that in the distance of $D = 0\,\mu m$, there are the highest efficiency and lowest insertion loss, but with increasing displacement, the insertion loss is increased and at $D = 10\,\mu m$ reaches its maximum. To compare different dimensions of the modulator, in Fig. 6(a) it seems that for the dimensions of $x = y = 1\,\mu m$ the insertion loss is very high, so even for the displacement of $D = 0\,\mu m$ this value reaches 0.9, and for $x = y = 5\,\mu m$ in Fig. 6(b) this value is about 0.5, while this amount is negligible for the dimension of $x = y = 10\,\mu m$ (Fig. 6(c)). In other words, with respect to the fiber core radius, by decreasing the modulator dimensions, losses increase dramatically which makes it difficult for modulator function. Now consider that the displacement between the fiber and the modulator is constant, the coupling efficiency and insertion loss versus the waveguide dimensions are plotted in Fig. 7. It is seen that with increasing waveguide dimensions, the value of insertion loss is decreased, and for dimensions of $10\,\mu m$ it is less than 0.1.

Now, having the light profile in the modulator, the effect of field formation on the main

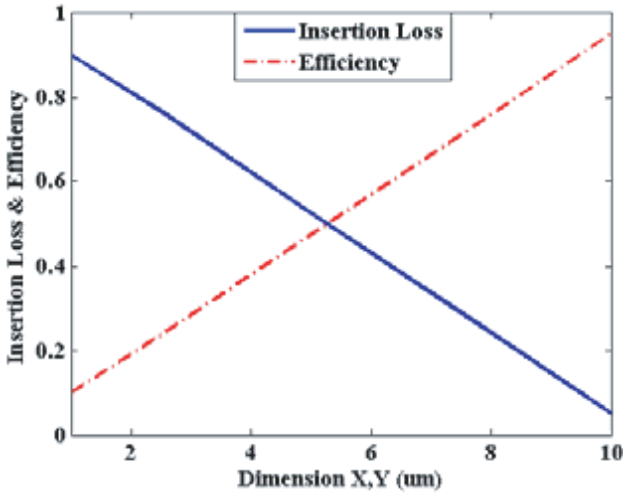

Figure 7. Coupling efficiency and insertion loss vs. the modulator dimensions for $D = 0.5\,\mu m$ refractive index of core and cladding for optical fiber are $n_1 = 1.46$ and $n_2 = 1.45$ and for waveguide are $n_1 = 2.3$ and $n_2 = 2.2$ respectively.

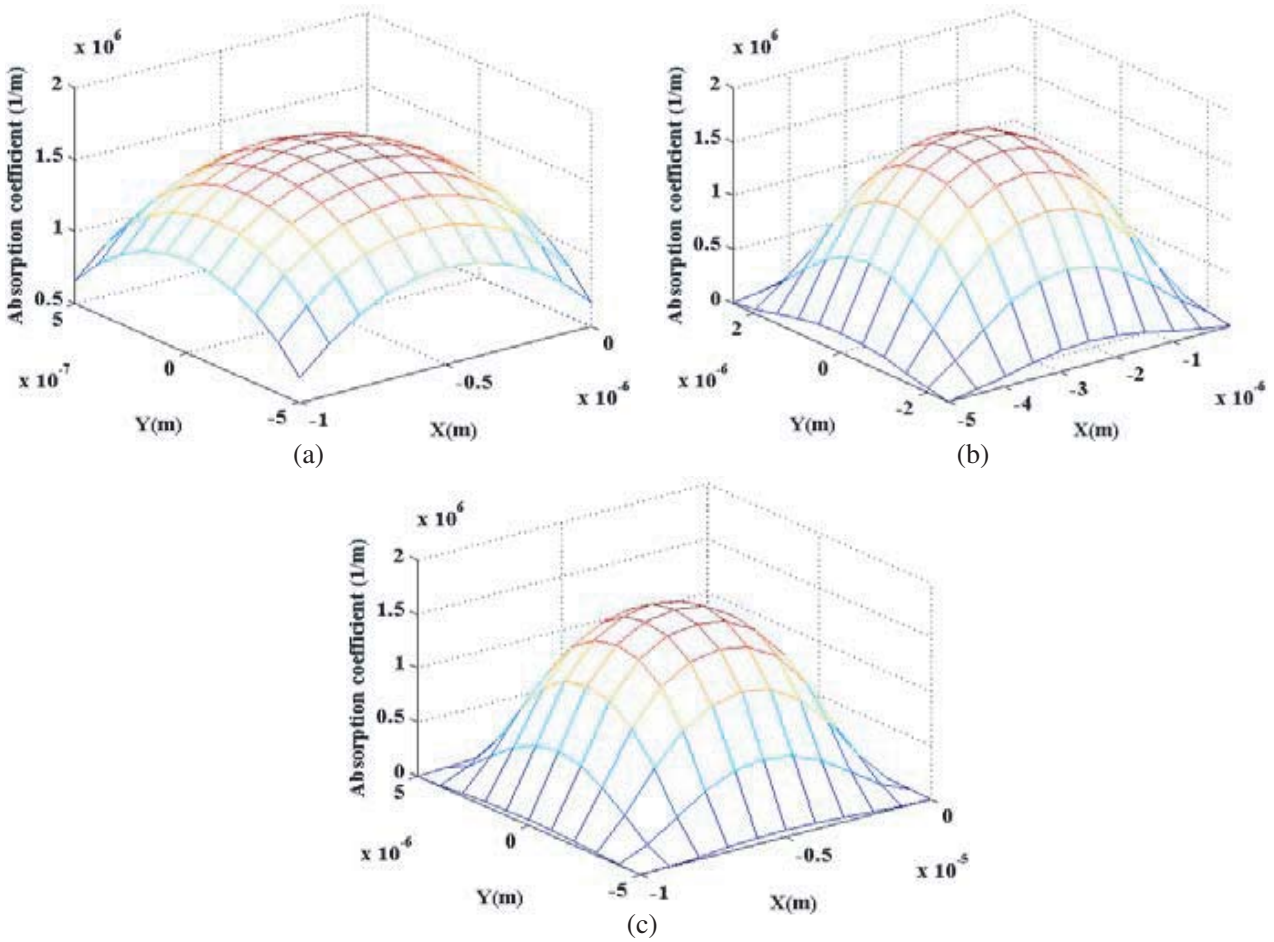

Figure 8. Absorption coefficient for waveguide dimensions: (a) $x = y = 1\,\mu m$, (b) $x = y = 5\,\mu m$, (c) $x = y = 10\,\mu m$, $I_{pump} = 5\times10^8$ (Wcm^{-2}), $I_{probe} = 1.7\times10^3$ (Wcm^{-2}) and $I_{control} = 1.2\times10^2$ (Wcm^{-2}). Periods of QD layers, density of carriers, Reflection, and temperature are, $N = 95$, $N_a = 8\times10^{18}$ (cm^{-3}), $R = \%10T = 300\,K$.

characteristics of the modulator is considerable. As the pump power has the main effect on modulator operation, by reducing the pump power toward the waveguide side walls, probe modulation will be disturbed. In Fig. 8 it is observed that the absorption becomes weak with decreasing the pump power along the waveguide side walls.

It is noticeable that in Fig. 8(a) the absorption coefficient is almost uniform in the channel waveguide with $x = y = 1\,\mu$m, but in Fig. 8(b) for dimension of $x = y = 5\,\mu$m the absorption is near zero by the side walls, and in the modulator with the dimensions of $10\,\mu$m, by approaching to the waveguide walls, the electric field becomes weak much more than other dimensions and reaches zero (Fig. 8(c)). Therefore, in a modulator with dimensions of $10\,\mu$m the pump intensity, near the walls, is very close to zero, so the probe absorption will reach zero. However in modulator with $x = y = 1\,\mu$m, the field and absorption are almost uniform in the waveguide. The absorption and transmission coefficient near the walls are presented vs. the dimensions of the modulator for different amounts: $x = y = 1,\ 2.5,\ 5,\ 7.5,\ 10\,\mu$m in Fig. 9. It should be noted that with increasing dimensions of the modulator, the absorption near the walls has dropped dramatically (Fig. 9(a)), and transmission coefficient goes up noticeably (Fig. 9(b)). This

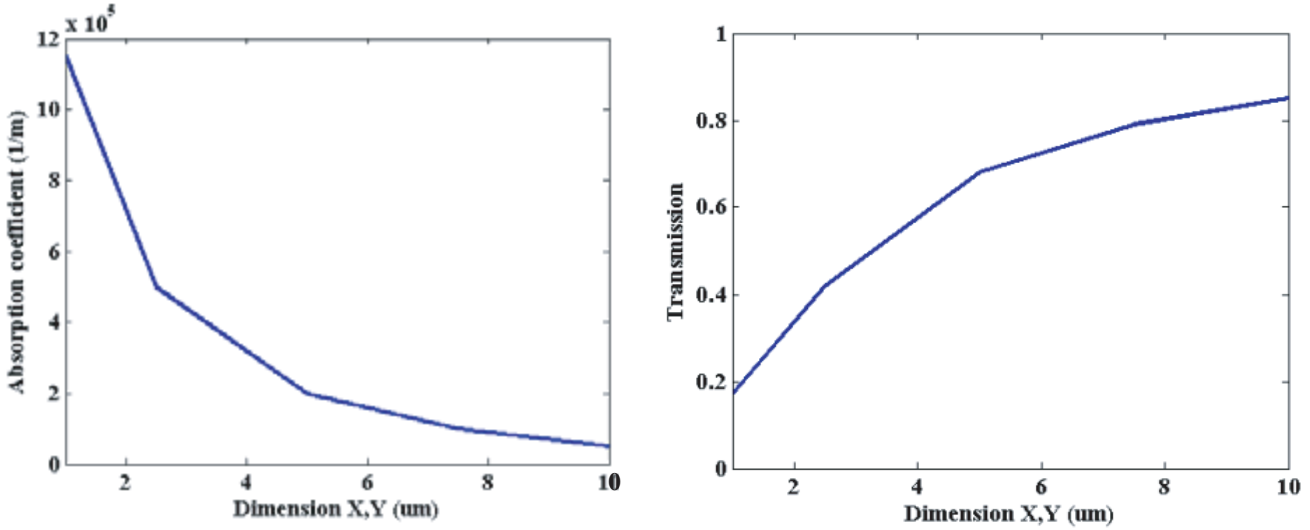

(a) (b)

Figure 9. (a) absorption and (b) transmission vs. the waveguide dimensions for different amounts: $x = y = 1,\ 2.5,\ 5,\ 7.5,\ 10\,\mu$m refractive index of core and cladding for optical fiber are $n_1 = 1.46$ and $n_2 = 1.45$ and for waveguide are $n_1 = 2.3$ and $n_2 = 2.2$ respectively.

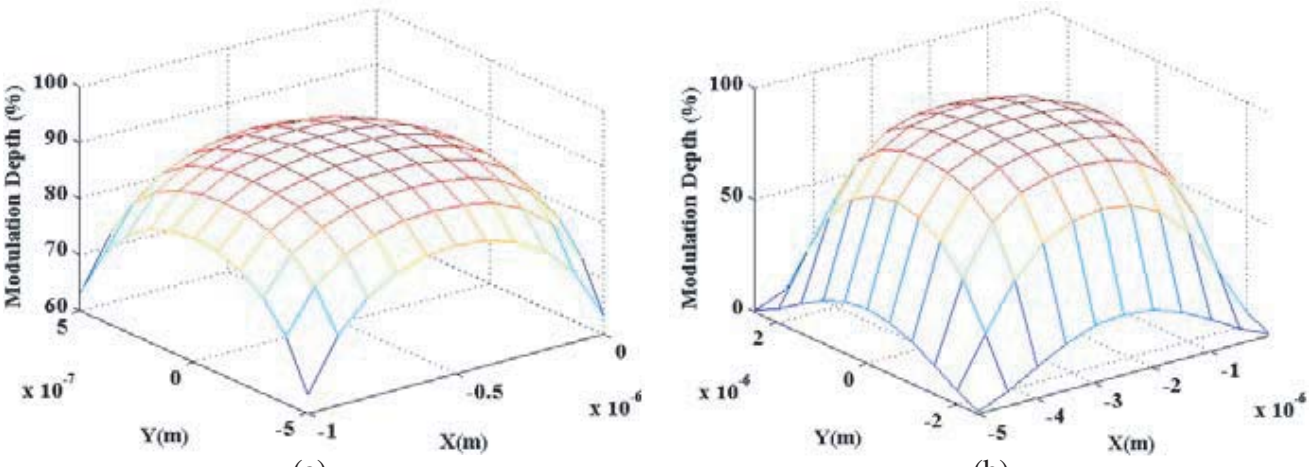

(a) (b)

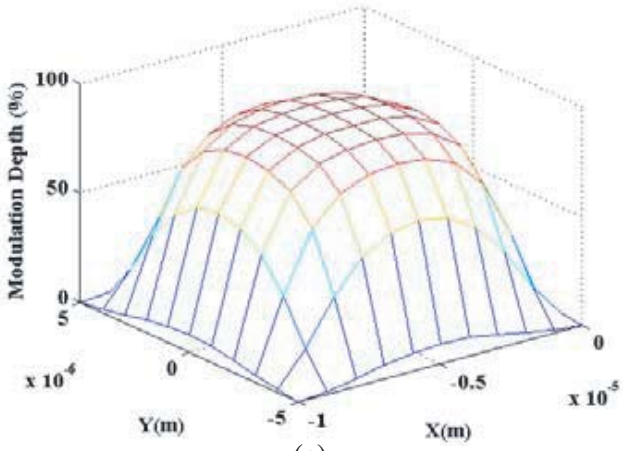

(c)

Figure 10. Modulation depth for dimensions: (a) $x = y = 1\,\mu\text{m}$, (b) $x = y = 5\,\mu\text{m}$, (c) $x = y = 10\,\mu\text{m}$, $I_{\text{pump}} = 5 \times 10^8$ (Wcm^{-2}), $I_{\text{probe}} = 1.7 \times 10^3$ (Wcm^{-2}) and $I_{\text{control}} = 1.2 \times 10^2$ (Wcm^{-2}). Periods of QD layers, density of carriers, Reflection, and temperature are, $N = 95$, $N_a = 8 \times 10^{18}$ (cm^{-3}), $R = \%10\, T = 300\,\text{K}$.

matter shows that modulator operation has high efficiency in the central region of the waveguide. The same situation is shown in Fig. 10 for depth of modulation. As we can see, with increasing dimensions of the modulator, the modulation depth decreases near the walls, and the modulation process uniformity becomes weak. One can see in Fig. 10(a) that the modulation depth is almost the same in the channel with $x = y = 1\,\mu\text{m}$, but in Fig. 10(b) for dimensions of $x = y = 5\,\mu\text{m}$, modulation depth becomes low near the side walls and for $x = y = 10\,\mu\text{m}$ is very weak at the corners (Fig. 10(c)). The depth of modulation vs. the channel size is shown in Fig. 11. The modulation depth decreases along the sides of the channel walls, and it reaches 10% for the dimensions of $10\,\mu\text{m}$, indicating modulator performance impairment in that area.

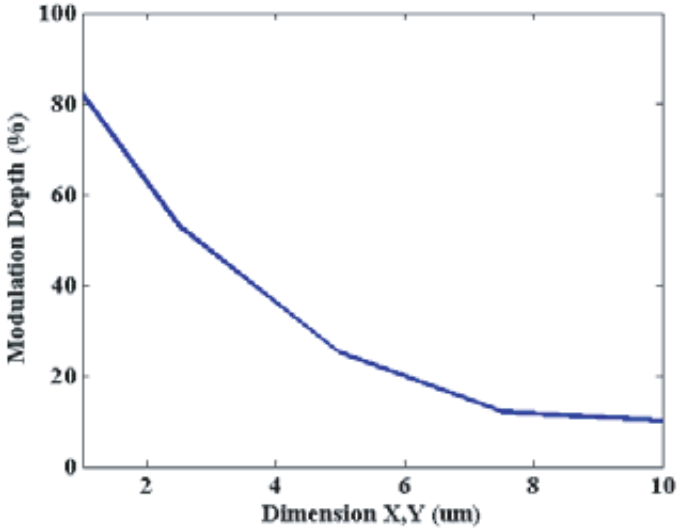

Figure 11. Modulation depth vs. the modulator dimension for different amounts: $x = y =$ 1, 2.5, 5, 7.5, $10\,\mu\text{m}$ refractive index of core and cladding for optical fiber are $n_1 = 1.46$ and $n_2 = 1.45$ and for waveguide are $n_1 = 2.3$ and $n_2 = 2.2$ respectively.

4. CONCLUSION

In this paper, proper characteristics of a waveguide as an all optical modulator are presented, and the roles of insertion loss and light profiles in the waveguide on the operation of the modulator including absorption and depth of modulation are considered. The effects of modulator dimensions on the insertion loss and light profile are also investigated, and some discussions are conducted on the appropriate dimensions. The results show that in modulator with dimensions of 1 µm, the light profile and consequently absorption and modulation process are uniform in the waveguide but give a significant increase in the insertion loss which disturbs the modulator performance. On the other hand, using a modulator with dimension of 10 µm, the modulation is not uniform, but insertion loss is negligible. So a modulator with dimensions of 10 µm will be a proper choice in contrast to other dimensions.

REFERENCES

1. Nevou, L., F. H. Julien, R. Colombelli, F. Guillot, and E. Monroy, "Room-temperature intersubband emission of GaN/AlN quantum wells at $\lambda = 2.3\,\mu m$," *Electron. Lett.*, Vol. 42, 1308–1309, 2006.
2. Hamazaki, J., S. Matsui, H. Kunugita, K. Ema, H. Kanazawa, T. Tachibana, A. Kikuchi, and K. Kishino, "Ultrafast intersubband relaxation and nonlinear susceptibility at 1.55 µm in GaN/AlN multiple-quantum wells," *Appl. Phys. Lett.*, Vol. 84, 1102–1104, 2004.
3. Friel, I., K. Driscoll, E. Kulenica, M. Dutta, R. Paiella, and T. D. Moustakas, "Investigation of the design parameters of AlN/GaN multiple quantum wells grown by molecular beam epitaxy for intersubband absorption," *J. Cryst. Growth*, Vol. 278, 387–392, 2005.
4. Nevou, L., M. Tchernycheva, L. Doyennette, F. H. Julien, E. Warde, R. Colombelli, F. Guillot, S. Leconte, E. Monroy, T. Remmele, and M. Albrecht, "New developments for nitride unipolar devices at 1.3–1.5 µm wavelengths," *Superlattices Microstruct.*, Vol. 40, 412–417, 2006.
5. Gopal, A. V., H. Yoshida, A. Neogi, N. Georgiev, T. Mozume, T. Simoyama, O. Wada, and H. Ishikawa, "Intersubband absorption saturation in InGaAs-AlAsSb quantum wells," *IEEE J. Quantum Electron.*, Vol. 38, 1515–1520, 2002.
6. Akimoto, R., B. S. Li, K. Akita, and T. Hasama, "Subpicosecond saturation of intersubband absorption in (CdS/ZnSe)/BeTe quantum well waveguides at telecommunication wavelength," *Appl. Phys. Lett.*, Vol. 87, 181104, 2005.
7. Sun, H. H., F. Y. Guo, D. Y. Li, L. Wang, D. B. Wang, and L. C. Shao, "Intersubband absorption properties of high Al content $Al_xGa_{1-x}N$/GaN multiple quantum wells grown with different interlayers by metal organic chemical vapor deposition," *Nanoscale Research Letters*, Vol. 7, 1–6, 2012.
8. Neogi, A., H. Yoshida, T. Mozume, N. Georgiev, and O. Wada, "Intersubband transition and ultrafast all-optical modulation using multiple InGaAs-AlAsSb-InP coupled double-quantum-well structures," *IEEE J. Sel. Top. Quantum Electron.*, Vol. 7, 7, 2001.
9. Chen, G., X. Q. Wang, X. Rong, P. Wang, F. J. Xu, N. Tang, Z. X. Qin, Y. H. Chen, and B. Shen, "Intersubband transition in GaN/InGaN multiple quantum wells," *Sci. Rep.*, Vol. 5, 11485, 2015.
10. Fu, H., Z. Lu, X. Huang, H. Chen, and Y. Zhao, "Crystal orientation dependent intersubband transition in semipolar AlGaN/GaN single," *App. Phys.*, Vol. 119, 174502, 2016.
11. Rostami, A., H. Baghban, and H. Rasooli Saghai, "An ultra-high level second-order nonlinear optical susceptibility in strained asymmetric GaN-AlGaN-AlN quantum wells: Towards all-optical devices and systems," *Microelectronics J.*, Vol. 38, 900, 2007.
12. Rahmani, A. and A. Rostami, "Ultrafast GaN/AlN modulator based on quantum dot for terabit all-optical communication," *Optik*, Vol. 125, 3844, 2014.
13. Kim, J., M. Laemmlin, C. Meuer, D. Bimberg, and G. Eisenstein, "Theoretical and experimental study of high-speed small-signal cross-gain modulation of quantum-dot semiconductor optical amplifiers," *IEEE J. of Quantum Electronics*, Vol. 45, 3, 2009.

14. Nishihara, H., M. Haruna, and T. Suhara, *Optical Integrated Circuits*, 29, 89, McGraw-Hill, USA, 1985.
15. Kawano, K. and T. Kitoh, *Introduction to Optical Waveguide Analysis*, John Wiley & Sons, Newyork, 37, 2001.